Performance Evaluation of Single-Phase Transfomer-less PV Inverter Topologies

Jinia Roy *, Yinglai Xia †, and Raja Ayyanar *
*School of Electrical and Computer Engineering
Arizona State University, Tempe, AZ 85287 USA
†Kilby Labs, Texas Instruments, Dallas, TX
E-mail: jinia.roy@asu.edu; yinglaixia@gmail.com; rayyanar@asu.edu

***Abstract*—Double line frequency power decoupling with reduced capacitance and mitigation of leakage current are two of the major challenges of any grid-connected single phase photovoltaic (PV) inverter. This paper compares the performances of different topologies for single phase transformer-less PV application in terms of the power decoupling capacitor requirement, the current ripple and total harmonic distortion (THD), efficiency performance, and leakage current. The topologies considered include a doubly grounded T-type dynamic dc-link (DDCL) inverter, a half-bridge voltage swing (HBVS) inverter, and conventional full-bridge (FB) inverter with three different modulation schemes (bipolar, hybrid, and unipolar). The leakage current arising from both parasitic capacitances of the PV module and the heat sink is considered in the present study which is essential for design of the electromagnetic interference (EMI) filters. The analysis are supported by experimental results from SiC-based 1 kW hardware prototypes operating at 120 V ac nominal output at a switching frequency of 100 kHz for each of the topology.**

***Index Terms*—Active power decoupling, common mode voltage, heat sink leakage current, PV array leakage current, parasitic capacitance, transformer-less PV inverter, THD.**

I. Introduction

With the increasing environmental concerns and growing energy demands, solar photovoltaic (PV) has gained significant attention among the renewable energy resources [1]. PV inverter is an integral part of both the utility and residential single phase grid-connected PV systems, which is responsible for extracting maximum power from the PV module and integrating it to the grid. The transformer-less implementation of PV inverters are preferred due to their advantages of reduced volume, higher efficiency, and lower cost. However, they have two implementation challenges which include the mitigation of the capacitively-coupled ground current [2]–[4] and like any other single phase rectifiers and inverters, the need of double line frequency power decoupling [5]–[10].

By active power decoupling method, the capacitance can be reduced to replace the less reliable electrolytic capacitor by an all-film capacitor implementation [11]–[14]. Also the high frequency common mode ground current can be mitigated or at least reduced by topological improvement like the doubly grounded structure, half-bridge (HB) derived converter, or adding a free wheeling path at certain switching interval of the operating cycle. However, the leakage current arising from the grounded heat sink still exists and its estimation is required to design the electromagnetic interference (EMI) filters for the PV inverters [15]. Improved efficiency, power density, and reduced total harmonic distortion (THD) with comparable inductor (power density is function of inductor volume) are other three important metrics to design the PV inverters.

This paper compares different topologies for transformer-less PV application in terms of the power decoupling capacitor requirement, the current ripple and THD, efficiency performance, leakage current, and number of circuit components. The leakage current arising from both parasitic capacitances of the PV module and the heat sink is considered in the present study. The topologies considered include a doubly grounded T-type dynamic dc-link inverter (DDCL), a HB derived voltage swing inverter, and conventional full-bridge (FB) inverter with three different modulation schemes (bipolar, hybrid, and unipolar). This paper is helpful for the researchers to choose the appropriate topology for transformer-less PV applications from the perspective of its cost and performance. A comprehensive analysis and experimental results are provided for 1 kW, 120 V ac nominal output at a switching frequency of 100 kHz for each of the topology compared.

The rest of the paper is organized as follows. Section II gives a detail of the leakage current present in PV inverters. The topologies which are considered for comparison in this paper are introduced in the following Section III. Detailed experimental results for a SiC-based 1 kW hardware prototype based on each of the topologies are provided in Section IV. Finally a conclusion of the presented work is drawn in Section V.

II. Leakage Current

A. PV module leakage current

For safety reasons, the frame of a PV module is required by codes to be grounded. This leads to a significant parasitic capacitances between the positive and negative PV terminals to the frame, and hence to the grid neutral. This parasitic capacitance of PV panel is proportional to the power rating. When the positive and/or negative terminals of the PV module are connected to a switching node of the inverter with respect to ground, it results in a significant high-frequency common mode ground current through these parasitic capacitances as in FB inverters with unipolar modulation scheme.

978-1-5386-1180-7/18/$31.00 ©2018 IEEE

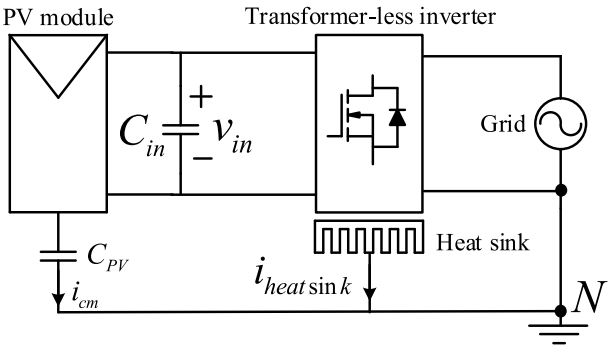

Fig. 1. Leakage.

TABLE I
COMPONENT DETAILS

Component	Parameters
C_1 , C_2 , C_3	12 μF/500 V (2), 30 μF/500 V
C_{link}	55 μF/500 V
L_b , L_{bb} , L_{inv}, L	210 μH
L_A , L_B	105 μH

Fig. 1 shows the leakage current i_{cm} flowing through the parasitic capacitance C_{PV} between the PV module and the ground. C_{PV} varies with the panel frame structure and the weather condition which typically ranges from 60-110 nF/kW in the standard PV modules and 100-160 nF/kW in the thin-film PV modules. For 1 kW application, the capacitance value used in this paper is 80 nF.

B. Heat sink leakage current

When a common heat sink for electrically insulated MOSFETs is grounded, a high-frequency leakage current $i_{heatsink_j}$ flows through the heat sink and parasitic capacitance C_{h_j} formed between j^{th} MOSFET drain tab to the heat sink. The measured value of this capacitance is around 200 pF for the SiC based experimental prototype with aluminum heat sink. $i_{heatsink}$ is given in (1) where V_{jN} is the voltage across the drain of j^{th} MOSFET and the grid neutral N, and n is the total number of active components. It is to be noted that the leakage current is a function of the switching frequency and the switch gate resistor R_g.

$$i_{heatsink} = \sum_{j=1}^{n} i_{heatsink_j} = \sum_{j=1}^{n} C_{h_j} \frac{dV_{jN}}{dt} \tag{1}$$

III. TRANFORMER-LESS PV INVERTER TOPOLOGIES

The grid voltage and grid current at an arbitrary power factor $\cos\theta$, with the corresponding instantaneous grid power are given in (2). As P_g has 120 Hz ripple component and power from PV is a pure dc, energy storage element is required for instantaneous power balance.

$$v_g = V_g \sin(\omega t); \quad i_g = I_g \sin(\omega t + \theta)$$
$$P_g = \frac{V_g I_g}{2} (\cos\theta - \cos(2\omega t + \theta)) \tag{2}$$

A. T-type dynamic dc-link inverter

The T-type doubly grounded dynamic dc-link inverter [16] as shown in Fig. 2a has an input boost stage followed by an asymmetric HB inverter stage. The inverter stage coupled with a bi-directional T-branch leading to three voltage level operation leading to a reduced THD and higher efficiency w.r.t. the one without the T-branch implementation. As the grid neutral is directly connected to the PV negative terminal mitigating the ground leakage current. A large average voltage and a large double line frequency voltage ripple on the dc-link v_{link} address the power decoupling with a much reduced capacitor value. (3) gives the expression for v_{link} where V_{avg} is the dc-link average and V_r is the magnitude of the ripple component. The required decoupling capacitance C_{link} is obtained from (4) where S_g is the VA rating of the converter.

$$v_{link} = V_{avg} + V_r \sin(2\omega t + \theta) \tag{3}$$

$$V_{avg} V_r C_{link} = \frac{V_g I_g}{4\omega} = \frac{S_g}{2\omega} \tag{4}$$

B. Half-bridge voltage swing inverter

The half-bridge voltage swing (HBVS) inverter [6], [12] as shown in Fig. 2b is comprised of an input boost stage (to address wide PV voltage variation under partial shading), an intermediate synchronous buck-boost stage (to address the power decoupling), and finally a half bridge inverter. The grid neutral is directly connected to the PV negative terminal through half bridge capacitor, which significantly reduces the capacitive ground current. A large sinusoidal swing of the HB capacitors v_1 and v_2 (shown in (5) are allowed along with a limited double line frequency voltage ripple on the dc-link v_3 (given in (6)) to address the power decoupling with a reduced capacitor value.

$$v_1 = \frac{v_3}{2} + A\sin(\omega t + \zeta); \qquad v_2 = \frac{v_3}{2} - A\sin(\omega t + \zeta) \tag{5}$$

$$v_{dc} = V_{avg} + V_r \sin(2\omega t + \theta) \tag{6}$$

where, $2A$ is the allowed peak-peak ripple of the HB capacitor voltages, ζ is their phase shift relative to the grid voltage, V is the DC-link average voltage, and V_r is the DC-link ripple voltage. The total ripple power supported by all the three capacitors C_1, C_2, and C_{dc} with the capacitance value given by (7). More detail discussions on its operating principles can be referred form [14].

$$V_{avg} V_r (2C_{dc} + C) + CA^2 = \frac{V_g I_g}{2\omega} = \frac{S_g}{\omega}$$
$$\zeta = \frac{\pi}{4} + \frac{\theta}{2} \tag{7}$$

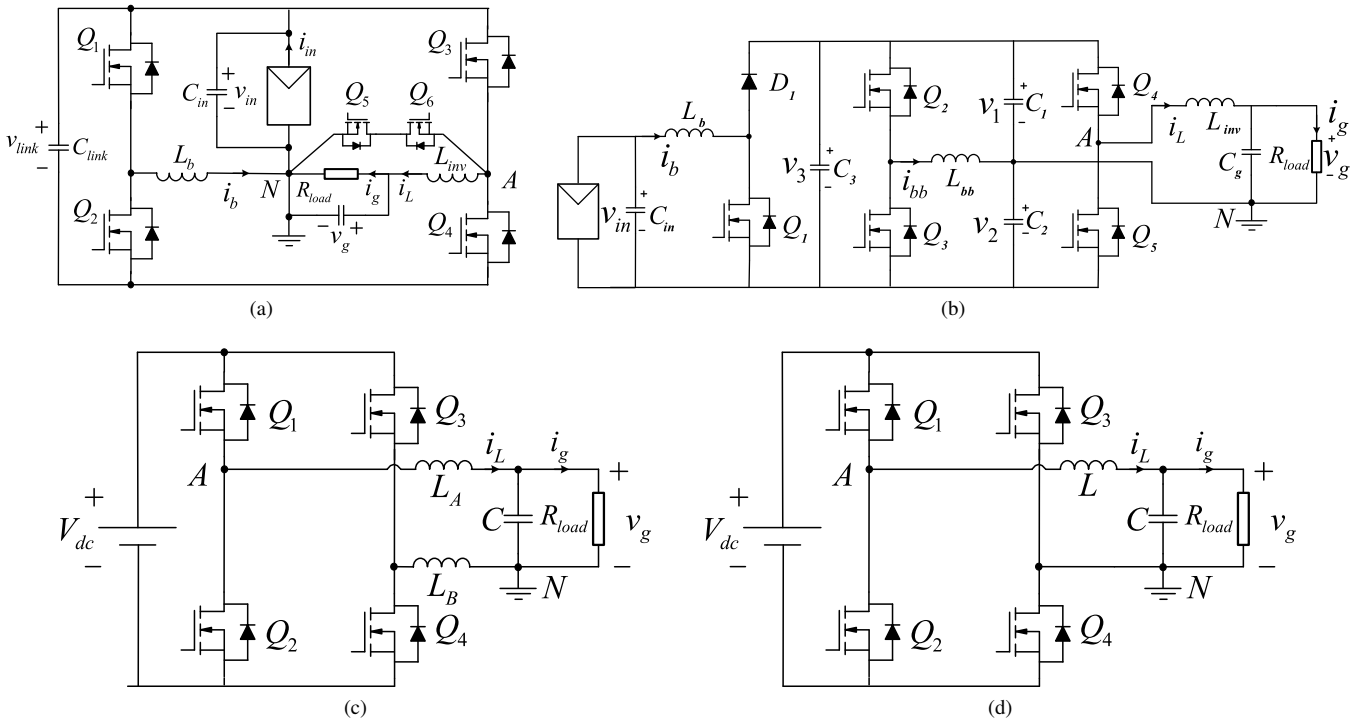

Fig. 2. Topologies considered for comparison for transformer-less PV application (a) T-type doubly grounded dynamic dc-link, (b) HBVS, (c) FB with bipolar and unipolar modulation, (d) FB with hybrid modulation.

C. Full-bridge inverter

Among many modulation methods available for FB inverters, bipolar pulse width modulation (PWM), hybrid PWM, and unipolar PWM are the three popular modulation schemes. In bipolar and unipolar schemes, all the four main switches are switching at the same carrier frequency. While in hybrid PWM, two of the four switches are driven by high switching frequency PWM signals for high quality sinusoidal output and the other two are commutated at line frequency, which reduces the inverter losses.

Two inductors are used for bipolar and unipolar schemes as shown in Fig. 2c to reduce the common mode leakage current. It is to be noted that no leakage current is ideally present for bipolar PWM scheme if the parameters of both the inductors are exactly matched. However, it is difficult to have an exact match, and leakage current is not negligible as is shown in experimental results in the next Section. Fig. 2d shows the circuit for hybrid scheme implementation with a single inductor. Power decoupling in all three cases is addressed by a large electrolytic capacitor at the dc-link, considering around 3% voltage ripple.

IV. Hardware implementation and experimental results

A. Hardware prototype and component details

The component details for 1 kW transoformer-less PV inverter topologies are given in Table I. The capacitors are selected based on the specified voltage and power decoupling requirement. The grid side inductors are designed to be same for all the topologies to have a fair comparisons of the corresponding THDs. The inductors are custom-made with E64/10/50-3F3 ferrite core and Litz wire for obtaining a lower profile design with lower condustion loss. All the prototypes are SiC-based with an integrated heat sink connected to the drain tab of the MOSFETs with thermal pad. The heat sink is grounded and $i_{heatsink}$ is the sum of the measured heat sink leakage current for all the switches together.

TABLE II
Converter Specification

Parameter	Rating
Output	120 V, 60 Hz, 1 kW
Switching frequency, f_{sw}	100 kHz

Avago ACPL 337J is used as the driver IC, with a negative voltage for a reliable device turn-off. The auxiliary power as required by the gate driver and controller section is derived externally. LeCroy 6200A oscilloscope is used to capture the relevant waveforms and power analyzer YOKOGAWA WT3000 is used to measure the efficiency.

B. Experimental results

Fig. 3 shows the steady state experimental results showing the basic waveforms for each of the topology at 1 kW, 120 V ac nominal output. For the unipolar PWM the presence of C_{PV} has significant influence on the efficiency and THD performance, so the results are also provided for unipolar

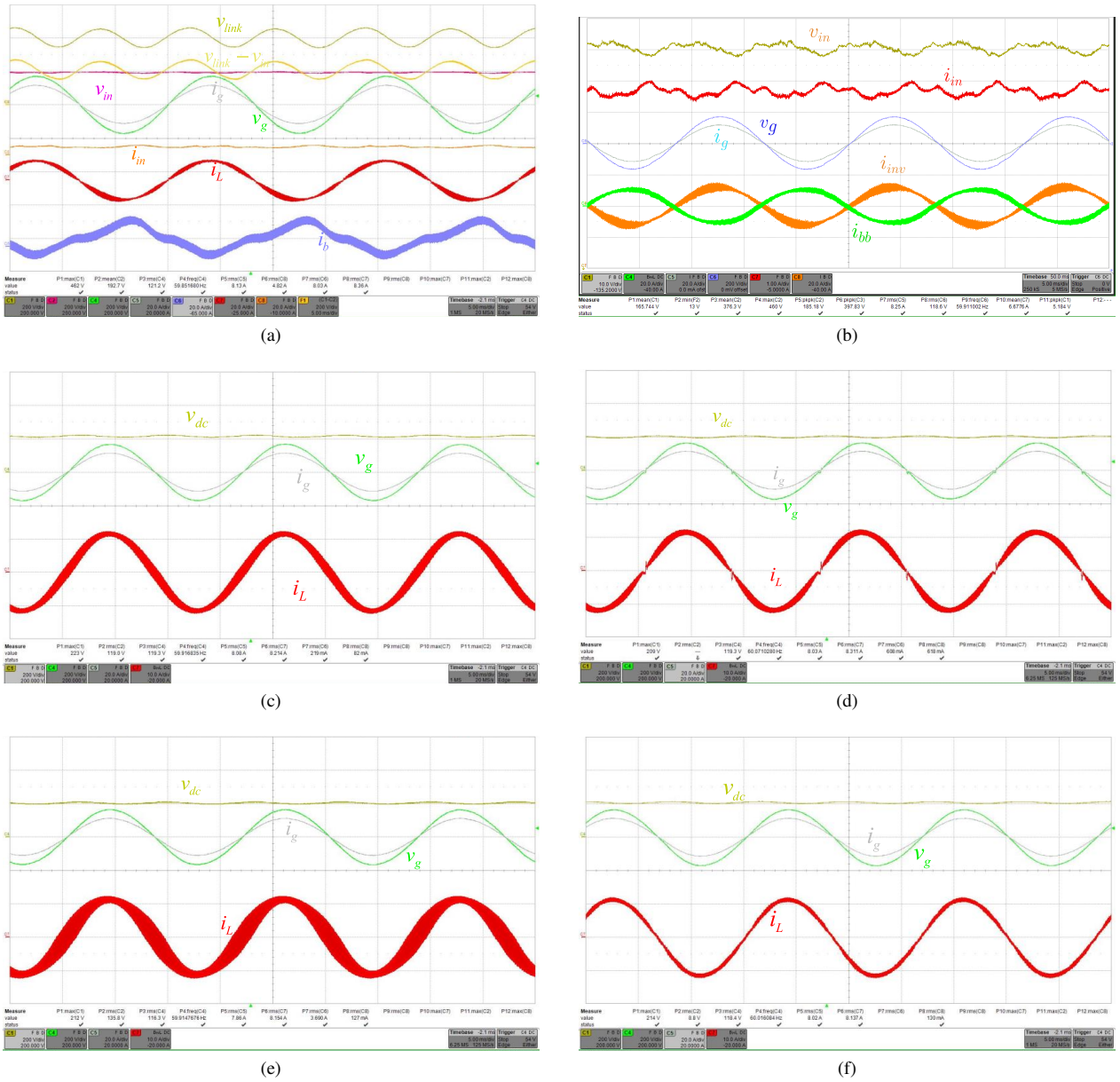

Fig. 3. Steady state experimental waveforms (time : 5 ms/div) for SiC based transformer-less PV inverter operating at nominal operating condition for (a) T-type dynamic dc-link (voltages: 200 V/div, currents: 20 A/div), (b) HBVS (v_{in}: 10 V/div, v_g: 200 V/div, i_{in}: 1 A/div, other currents: 20 A/div), (c) FB with bipolar modulation, (d) FB with hybrid modulation, (e) FB with unipolar modulation and with C_{pv} , (f) FB with unipolar modulation and without C_{pv} (voltages: 200 V/div, i_g: 20 A/div, i_L: 10 A/div).

PWM without C_{PV}. Fig. 4 gives the leakage current (i_{cm}, $i_{heatsink}$), common mode voltage v_{cm}, and voltage across the drain and the grid neutral for one switch (v_{AN}) which can be referred from Fig. 2. Table III gives the detail of all the parameters under consideration for each of the topology. Efficiency is measured at rated condition.

It can be noted that i_{cm} is dependent on the topology and modulation scheme, where i_{cm} for T-type $<$ HBVS $<$ bipolar $<$ hybrid $<$ unipolar. As expected, $i_{heatsink}$ depends on the number of switches and the switching voltage across the MOSFETs drain to the grid neutral, where $i_{heatsink}$ for bipolar $\approx$ hybrid $\approx$ unipolar $<$ T-type $\approx$ HBVS. THD is related to the voltage levels and effective switching frequency, unipolar $<$ T-type $\approx$ hybrid $<$ HBVS $\approx$ bipolar.

V. Conclusion

This paper compares the performances of different topologies for single phase transformer-less PV application in terms of the power decoupling capacitor requirement, the current ripple and total harmonic distortion (THD), efficiency performance, and leakage current. The common mode current is dependent on the topology and modulation scheme; in doubly

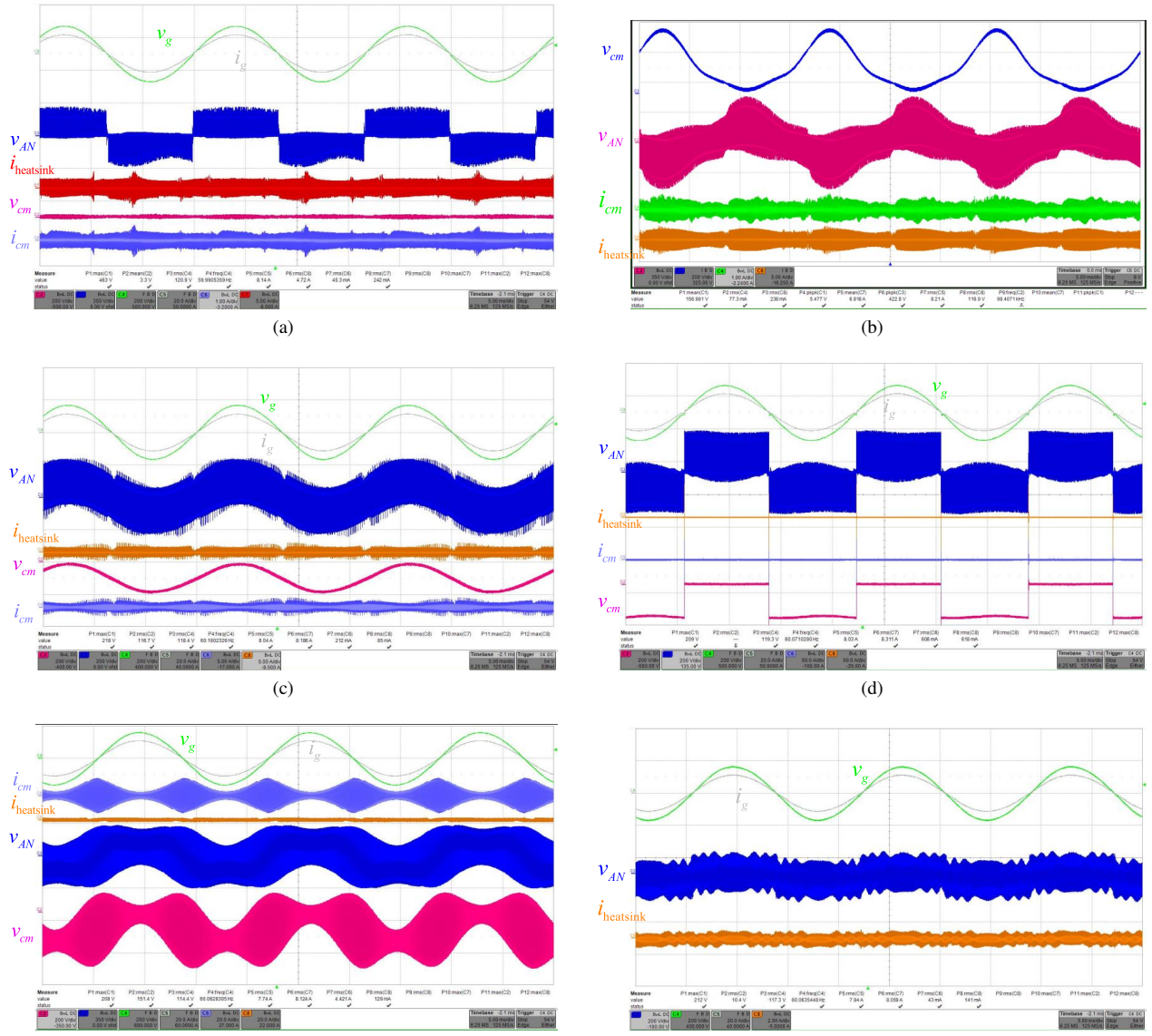

Fig. 4. Experimental waveforms (v_g: 200 V/div, i_g: 20 A/div, time : 5 ms/div) showing the leakage currents (i_{cm}, $i_{heatsink}$), voltage across the drain and the grid neutral for one switch (v_{AN}), and common-mode voltage (v_{cm}) for (a) T-type dynamic dc-link, (b) HBVS (v_{cm}: 200 V/div, i_{cm}: 1 A/div, v_{AN}: 350 V/div, $i_{heatsink}$: 5 A/div), (c) FB with bipolar modulation (voltage: 200 V/div, current: 5 A/div), (d) FB with hybrid modulation (voltage: 200 V/div, current: 50 A/div), (e) FB with unipolar modulation and with C_{pv} (voltage: 200 V/div, current: 5 A/div), (f) FB with unipolar modulation and without C_{pv} (v_{cm}: 200 V/div, v_{AN}: 350 V/div, current: 20 A/div).

TABLE III
COMPARISON OF TRANSFORMER-LESS PV INVERTER TOPOLOGIES

Parameter	**T-type**	**HBVS**	**Bipolar FB**	**Hybrid FB**	**Unipolar with C_{pv}**	**Unipolar w/o C_{pv}**
Power decoupling	55 μF/ 500 V	54 μF/ 500 V	Large electrolytic cap in mF range			
THD (%)	6.7	11.6	10.1	6.5	31.7	3.5
Efficiency (%)	97	94.5	97	98	95.8	97.1
i_{cm} (mA)	45	77	212	618	4400	-
$i_{heatsink}$ (mA)	242	238	85	608	129	141
Active components	6 S	5 S, 1 D	4 S			

grounded it is mostly eliminated whereas, FB with unipolar it is significantly high which also affects the converter's THD and efficiency performance. The leakage current from the heat sink is dependent on the number of switches and the switching voltage across the MOSFETs drain to the grid neutral. The analysis are supported by experimental results from SiC-based 1 kW hardware prototypes operating at 120 V ac nominal output at a switching frequency of 100 kHz for each of the topology.

ACKNOWLEDGMENT

The work presented herein was funded in part by the Office of Energy Efficiency and Renewable Energy (EERE), U.S. Department of Energy, under Award Number DE-EE0006521 with North Carolina State University, PowerAmerica Institute. The authors would like to thank the institute for funding.

DISCLAIMER

REFERENCES

[1] P. Denholm, R. Margolis, T. Mai, G. Brinkman, E. Drury, M. Hand, and M. Mowers, "Bright future: Solar power as a major contributor to the U.S. grid," *IEEE Power and Energy Magazine*, vol. 11, no. 2, pp. 22–32, March 2013.

[2] Ó. López, F. D. Freijedo, A. G. Yepes, P. Fernández-Comesaña, J. Malvar, R. Teodorescu, and J. Doval-Gandoy, "Eliminating ground current in a transformerless photovoltaic application," *IEEE Transactions on Energy Conversion*, vol. 25, no. 1, pp. 140–147, March 2010.

[3] T. K. S. Freddy, N. A. Rahim, W. P. Hew, and H. S. Che, "Comparison and analysis of single-phase transformerless grid-connected pv inverters," *IEEE Transactions on Power Electronics*, vol. 29, no. 10, pp. 5358–5369, Oct 2014.

[4] T. Kerekes, R. Teodorescu, M. Liserre, C. Klumpner, and M. Sumner, "Evaluation of three-phase transformerless photovoltaic inverter topologies," *IEEE Transactions on Power Electronics*, vol. 24, no. 9, pp. 2202–2211, Sept 2009.

[5] Y. Xia, J. Roy, and R. Ayyanar, "A capacitance-minimized, doubly grounded transformer less photovoltaic inverter with inherent active-power decoupling," *IEEE Transactions on Power Electronics*, vol. 32, no. 7, pp. 5188–5201, July 2017.

[6] J. Roy, Y. Xia, and R. Ayyanar, "A single phase transformerless string inverter with large voltage swing of half-bridge capacitors for active power decoupling," in *2016 IEEE Energy Conversion Congress and Exposition (ECCE)*, Sept 2016, pp. 1–7.

[7] R. Chen, Y. Liu, and F. Z. Peng, "DC capacitor-less inverter for single-phase power conversion with minimum voltage and current stress," *IEEE Transactions on Power Electronics*, vol. 30, no. 10, pp. 5499–5507, Oct 2015.

[8] Y. Xia, J. Roy, and R. Ayyanar, "A gan based doubly grounded, reduced capacitance transformer-less split phase photovoltaic inverter with active power decoupling," in *2017 IEEE Applied Power Electronics Conference and Exposition (APEC)*, March 2017, pp. 2983–2988.

[9] P. T. Krein, R. S. Balog, and M. Mirjafari, "Minimum energy and capacitance requirements for single-phase inverters and rectifiers using a ripple port," *IEEE Transactions on Power Electronics*, vol. 27, no. 11, pp. 4690–4698, Nov 2012.

[10] J. Roy, Y. Xia, and R. Ayyanar, "Gan-based high gain soft switching coupled-inductor boost converter," in *2017 IEEE Energy Conversion Congress and Exposition (ECCE)*, Oct 2017, pp. 1687–1693.

[11] L. C. Breazeale and R. Ayyanar, "A photovoltaic array transformer-less inverter with film capacitors and silicon carbide transistors," *IEEE Transactions on Power Electronics*, vol. 30, no. 3, pp. 1297–1305, March 2015.

[12] J. Roy, Y. Xia, and R. Ayyanar, "Sliding mode control of a single phase transformer-less pv inverter with active power decoupling," in *2017 IEEE Energy Conversion Congress and Exposition (ECCE)*, Oct 2017, pp. 23–29.

[13] I. Serban, "Power decoupling method for single-phase H-Bridge inverters with no additional power electronics," *IEEE Transactions on Industrial Electronics*, vol. 62, no. 8, pp. 4805–4813, Aug 2015.

[14] J. Roy and R. Ayyanar, "A single phase transformer-less string inverter with integrated magnetics and active power decoupling," in *2017 IEEE Applied Power Electronics Conference and Exposition (APEC)*, March 2017, pp. 3601–3607.

[15] H. Akagi and T. Doumoto, "A passive emi filter for preventing high-frequency leakage current from flowing through the grounded inverter heat sink of an adjustable-speed motor drive system," *IEEE Transactions on Industry Applications*, vol. 41, no. 5, pp. 1215–1223, Sept 2005.

[16] Y. Xia, J. Roy, and R. Ayyanar, "A high performance t-type single phase double grounded transformer-less photovoltaic inverter with active power decoupling," in *2016 IEEE Energy Conversion Congress and Exposition (ECCE)*, Sept 2016, pp. 1–7.